DOI: 10.1002/adem.200800123

In-Situ Precipitated Nanocrystal Beneficial to Enhanced Plasticity of Cu-Zr Based bulk Metallic Glasses**

By *Lincai Zhang, Feng Jiang,* Dehong Zhang, Lin He, Jun Sun, Jitang Fan* and *Zhefeng Zhang*

Bulk metallic glass (BMG) possesses high strength, hardness and elastic deformation limit[1–3] and has long been regarded as a potential structural material. However, monolithic BMGs usually exhibit poor ductility and strain hardening ability during room temperature deformation due to highly localized shear bands, which significantly limits the range of possible applications. In order to overcome the limited plastic deformability of BMGs, Zr-, Cu- and Ti-based BMG composites with enhanced compression plasticity have been prepared by *ex-situ* or *in situ* methods.[4–9] Recent works also show that impressive improvements in plasticity can be achieved for some Zr-,[10] Pd-,[11] Pt-[12] and Cu-Zr-[13–21] based BMGs. In particular, Cu-Zr (or Zr-Cu) based BMGs such as $Cu_{50}Zr_{50}$,[13,14] $Cu_{47.5}Zr_{47.5}Al_5$ or $Zr_{47.5}Cu_{47.5}Al_5$),[15–17] $Cu_{46}Zr_{47}Al_7$,[18–19] $Zr_{65}Al_{7.5}Cu_{27.5}$[20] and $Cu_{50}Zr_{43}Al_7$,[21] have exhibited large compressive plastic strain. Moreover, these Cu-Zr based alloys are free of nocuous elements like Ni, Be and might be more suitable for biomedical and structural applications. The presence of samll nanocrystals, and the deformation-induced nanocrystallization have been given for factors contributing to the intrinsic ductility of these Cu-Zr based BMGs.[13–21] For example, it was considered that the large plasticity and strain hardening-type phenomena observed in $Cu_{47.5}Zr_{47.5}Al_5$ BMG were attributed to the chemical heterogeneities and Cu-rich nanocrystals with the size of about 5 nm.[15–16] The excellent plasticity of $Cu_{50}Zr_{50}$ and $Zr_{65}Al_{7.5}Cu_{27.5}$ alloy is also thought to be related with the presence of small nanocrystals.[13–14,20] Besides, the recent work of Kumar et al[17] shows that the heterogeneities observed in $Cu_{47.5}Zr_{47.5}Al_5$ alloy BMGs[15-16] were merely caused by transition electron microscope (TEM) during sample preparation and the deformation-induced nanocrystallization in the shear bands during compression was the main reason for the enhanced plasticity. Kim et al also claimed that some Cu-Zr based BMGs can display excellent plasticity due to the deformation-induced nanocrystallization during quasistatic compression.[21] And they also proposed that the plasticity of Cu–Zr containing glassy matrix was concerned with the activation energy for crystallization.[22] It is obvious that the origin of enhanced plasticity for Cu-Zr based alloys under quasistatic compression is still unclear and it is of great importance to clarify it. It should be noted that the geometrical imperfections in the compression specimen (i.e. miscut or non-orthogonal specimens) have great effects on the measured plastic strain during the compression test.[23] Thus, the three point bending test is better to evaluate the plasticity of BMGs.[24] Then, in this paper, a series of $Cu_{46}Zr_{47}Al_7$ alloys with different microstructures, including full glassy structure, marginal BMG containing small in-situ precipitated nanocrystals and BMG composite containing large CuZr crystals were prepared. Both compression and bending tests were undertaken to evaluate their plasticity. The effect of the nanocrystals on the plasticity of Cu-Zr based BMG and its composites were systematically investigated.

In this study, the tilt casting method in an arc furnace[25] was used to prepare BMG and its composites. Meantime, electromagnetic stirring function was introduced to the equipment by adding a current loop under the water-cooled copper crucible.[26] The alloy ingots with the nominal compositions $Cu_{46}Zr_{47}Al_7$ (at.%) were prepared by arc melting the mixtures of ultrasonically cleansed Zr (crystal bar, 99.9 at.%), Cu (99.99 at.%) and Al (99.99 at.%) pieces. The arc melting was performed in a Ti gettered high purity argon atmosphere. Each ingot was re-melted at least four times and the electromagnetism stirring was used in order to ensure the

[*] *Dr. L. C. Zhang, Dr. F. Jiang, Mr. D. H. Zhang, Prof. L. He, Prof. J. Sun*
State Key Laboratory for Mechanical Behavior of Materials
Xi'an Jiaotong University
Xi'an 710049, (P.R.China)
E-mail: jiangfeng@mail.xjtu.edu.cn
J. T. Fan, Prof. Z. F. Zhang
Shenyang National Laboratory for Materials Science
Institute of Metal Research
Chinese Academy of Sciences
72 Wenhua Road, Shenyang, 110016, (P.R.China)

[**] *The financial support from the National Natural Science Foundation of China (NSFC) under Grant Nos. 50501017 and 50671076 are gratefully acknowledged. The authors also wish to express their special thanks for the support from the National Basic Research Program of China (Grant No. 2004CB619303). Z.F.Z. would like to acknowledge financial support by the National Outstanding Young Investigator Grant of China under Grant No. 50625103. This work was also supported by Program for Changjiang Scholars, Innovative Research Team in University (PCSIRT) and the Program for New Century Excellent Talents in University (China).*

 © 2008 WILEY-VCH Verlag GmbH & Co. KGaA, Weinheim WILEY InterScience DISCOVER SOMETHING GREAT

COMMUNICATIONS

chemical homogeneity. Finally, by copper mold casting, the ingots were cast into plates with dimensions of 50 × 20 × h mm^3 (h = 1.5, 2 and 2.5). The different thickness h leads to different cooling rate upon solidification for the casting BMG plates. The as-cast alloys were characterized by X-ray diffraction (Rigaku D/MAX-RB, Cu-K_α radiation), differential scanning calorimetry (Setaram DSC 2000), scanning electron microscope (SEM JEOL S2700), and transmission electron microscope (JEOL Ltd. JEM2100F). The TEM (HRTEM) samples were obtained from the $Cu_{46}Zr_{47}Al_7$ alloy with 2.0 mm thickness at three different parts with the different cooling rates. They are about 0.1, 0.5 and 1.0 mm away from surface and signed them as A, B and C, respectively, as schematically illustrated in Figure 1. And for the alloys with 1.5 and 2.5 mm thickness, both of their TEM samples were obtained from the center parts, where the cooling rate was the lowest comparing with the other parts of the same plate. During the TEM preparation, firstly, 0.6 mm strips were cut at different part of the as cast plates with Electron Discharge Machining. Secondly, the 0.6 mm stripes were mechanically grind down to about 100 μm and measurement was taken to ensure the TEM observation location is basic in the middle of the thinned strips. Thirdly, a punch was used to cut 3 mm diameter disks from the thinned strip. Fourthly, the disk samples were again manually thinned to about 40 μm. Finally, TEM (HRTEM) samples were prepared using standard twin-jet electropolishing in a 20 vol.% solution of nitric acid in ethanol under the condition of 50 V, 30 mA, –40 °C. It should be noted that, crystallization can be introduced into metallic amorphous by improper ion milling preparation.[17,27] Here, electropolishing method was used to avoid such effect on the microstructures.

The samples for the compressive tests of $Cu_{46}Zr_{47}Al_7$ alloys were machined into different dimensions of 1.3 × 1.3 × 2.6, 1.8 × 1.8 × 3.6, 2.2 × 2.2 × 4.4 mm^3 for the 1.5, 2.0 and 2.5 mm plates, respectively. The compressive deformation was conducted on a computed-controlled, servo-hydraulic MTS 810 testing machine at a strain rate of about 1×10^{-4} s^{-1} at room temperature. The samples for the three-point bending tests of 1.5, 2.0 and 2.5 mm plates were all machined into the same dimensions of 20 × 4 × 0.8 mm^3 by symmetric milling from two surface sides to center. The bending test was conducted on a computed-controlled SANS testing machine at a displacement rate of 0.02 mm min^{-1} at room temperature. The span was 10 mm. During testing, the load-deflection ($R \sim \delta$) curves were recorded. The tensile surface under bending was previously polished in order to observe the shear band with SEM after test.

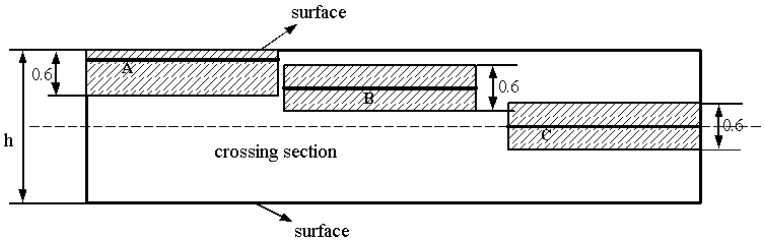

Fig. 1. Schematic representation of TEM sample site.

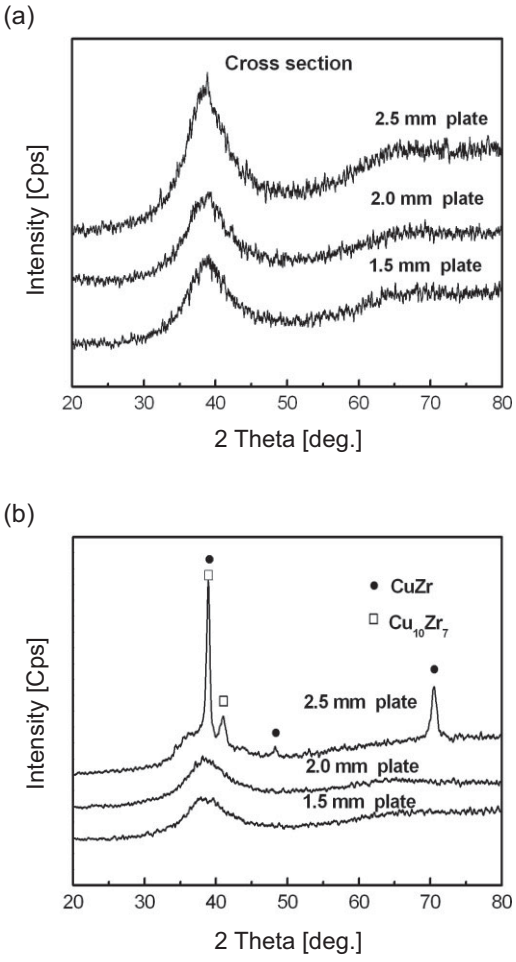

Fig. 2. XRD patterns of $Cu_{46}Zr_{47}Al_7$ alloys with different thickness cross section (b) center part of plates.

Figure 2(a) shows the X-ray diffraction (XRD) patterns recorded from the cross section of the as-cast alloys. For the 1.5 and 2.0 mm plates, both of the patterns consist of only a series of broad diffraction maxima without any detectable sharp Bragg peak, as it is characteristic for a glassy structure. However, a few of "spikes" were detected on the patterns of the 2.5 mm plate, indicating that some crystals have precipitated, which is due to the decrease in cooling rate with increase in thickness. Besides, the halves of plates in thickness were removed and the rest surfaces (center of plates, where the cooling rate is the lowest among the whole plate) were also measured by XRD and the results were shown in Figure 2(b). The patterns of the 1.5 and 2.0 mm plates are similar to the results from their cross sections. However, for the 2.5 mm plate, some crystalline diffraction peaks superimposed on the broad amorphous diffraction peak, were clearly identified as CuZr phase. Similar

 © 2008 WILEY-VCH Verlag GmbH & Co. KGaA, Weinheim

diffraction peaks have also been found in the $Zr_{48.5}Cu_{46.5}Al_5$ alloy.[28] Above XRD results indicate that the distribution of microstructures is not uniform due to the difference in cooling rate from the surface to the center. Moreover, the following TEM observation will also confirm the heterogeneities.

The bright field (BF) TEM images and the corresponding selected area electron diffraction (SAED) patterns (insets) as well as high resolution electron microscope (HREM) images of 2.0 mm plate at different parts were given in Figure 3(a–f). One can find that there is an obvious microstructure transition from A to B and C, which is corresponding to the decrease in cooling rate: no any detectable nonacrystals in the Part A, some tiny nanocrystals with size of about 5 nm in the Part B, and some nanocrystals with size less than 30 nm in the Part C. The HREM image (as shown in Fig. 3(b)) further demonstrates that Part A is fully amorphous without any visible nanocrystals, where mazelike clusters, which is the typical feature of metallic glasses, as widely observed before. Similarly, the HREM images (as shown in Fig. 3(d) and (f)) confirm the existence of nonacrystals in Parts B and C. Further TEM analysis confirms that these crystals are CuZr compound, which has a bcc-based B2 structure, with the lattice constant of a = 3.254 Å. Similar CuZr compound could also be found in other Cu-Zr-Al alloys.[28,29] Figure 3(g) and (h) show that there are a large number of crystals in the center part of 2.5 mm plate, which is consistent with its XRD result. The TEM analysis confirms that these crystals are main CuZr compound, which is agreement with the XRD results in Figure 2(b). For the 1.5 mm plate, its microstructure is similar to that of part A in 2.0 mm plate and it has fully glassy structure (not given). The above results of XRD and TEM (HRTEM) observations clearly indicated that the distribution of crystal-

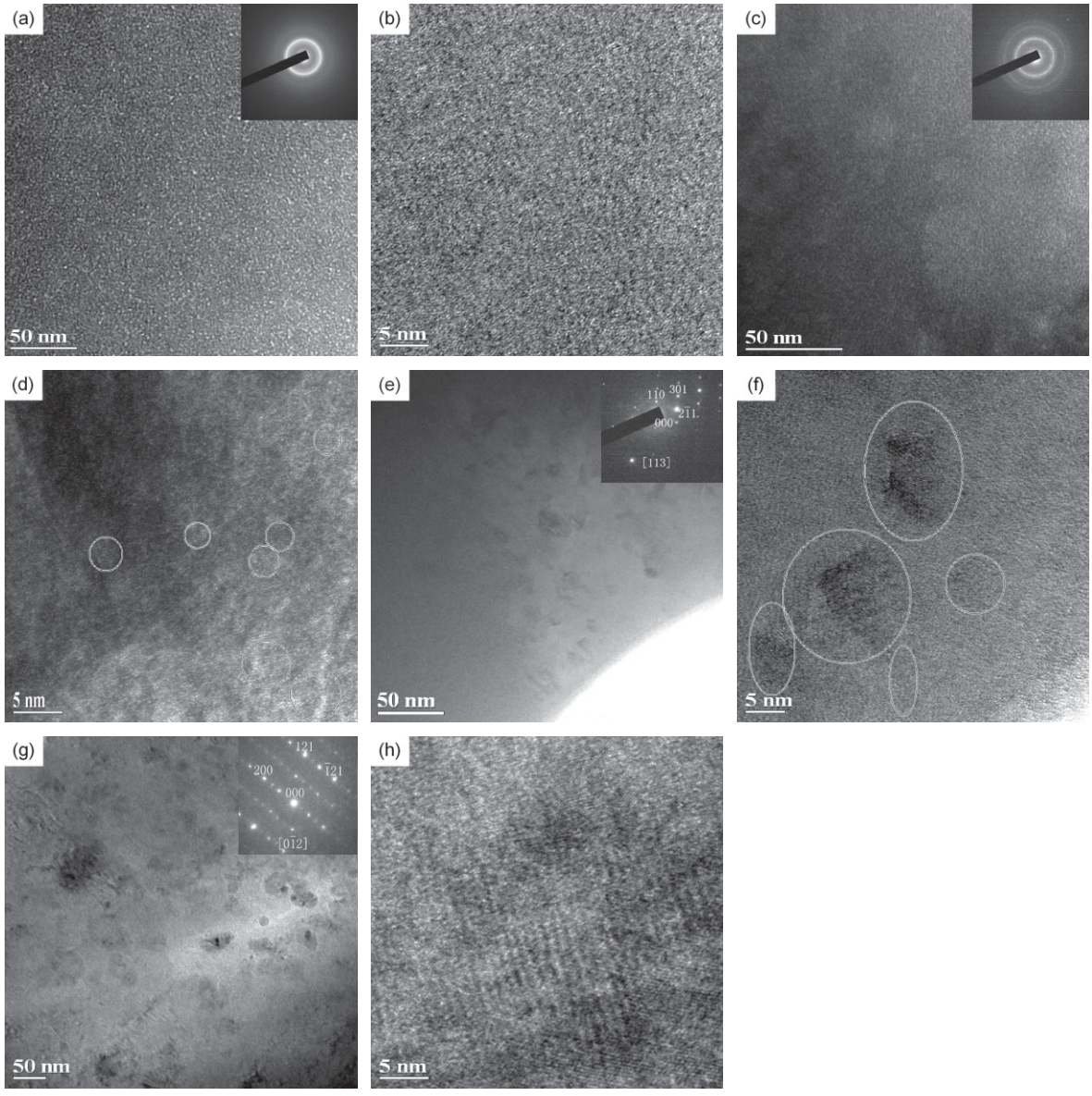

Fig. 3. The bright field (BF) TEM images and the corresponding selected area electron diffraction (SAED) patterns (insets) as well as high resolution electron microscope (HREM) images Bright-field TEM micrographs (a)–(f) for Part A, B and C in 2 mm $Cu_{46}Zr_{47}Al_7$ BMG and (g–h) center of 2.5 mm $Cu_{46}Zr_{47}Al_7$ alloy.

 © 2008 WILEY-VCH Verlag GmbH & Co. KGaA, Weinheim

line phase is not uniform due to the difference in cooling rate from the surface to the center.

The volume fractions of crystalline phases in the alloys can be evaluated by calculating the ratio of the heat release during annealing to the total crystallization enthalpy of the fully glassy alloy from DSC curves, i.e.

$\%V_{crys}=(\Delta H_{max}-\Delta H)/\Delta H_{max}$,[30] Where ΔH_{max} is the total enthalpy of transformation from the fully amorphous alloy to the completely crystallized alloy and ΔH is from the tested samples. The DSC profiles of plates in different thickness are shown in Figure 4(a). The crystallization enthalpy, ΔH were estimated through measuring the area of the crystallization peak and sample mass. These are 59.7, 58.0 and 56.0 J/g, for 1.5, 2.0 and 2.5 mm plates, respectively. According to the results of XRD and DSC, it can be thought that the 1.5 mm plate has fully glassy structure, and its volume fraction of crystalline phases is close to zero. The 2.0 and 2.5 mm plates are composites, which are main glassy structures with small volume fractions of crystalline phases of about 3.3 % and 6.7 %, respectively. It should be noted that the samples for the DSC were cut from the cross section and the volume fractions of crystalline phases obtained should be the same as that in the whole plate. In addition, the activation energy for crystallization of 1.5 mm amorphous plate was estimated by Kissinger's method, according to the DSC traces obtained at different heating rates of 5, 10, 15 and 40 K/min, respectively (see Fig. 4(b)). The result is about 344 kJ/mol, where the temperatures of the peak, T_p were used to calculate the data.

Figure 5(a) presents the compressive engineering stress-strain curves for the alloys investigated. The 1.5 mm plate sample with fully glassy structure yields at a stress about 1900 MPa and fails with poor plastic strain of about 1.2 %. The 2.0 mm plate sample yields at a stress of about 1894 MPa and fails at a stress of up to 2250 MPa. Besides, it exhibits apparent "work hardening" with significant plastic strain up to 6 %. Comparing with these of the 2.0 mm plate sample, the yield and fracture strengths of the 2.5 mm plate sample with more crystalline phases decrease. And its plastic strain to fracture is only about 3.0 %.

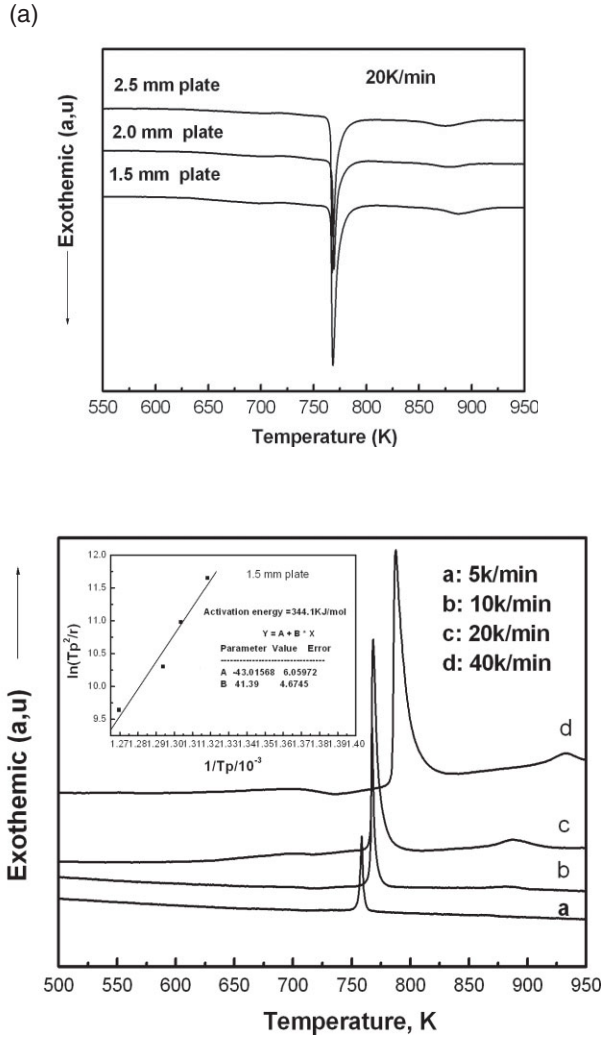

Fig. 4. (a) DSC traces of $Cu_{46}Zr_{47}Al_7$ alloys with different thickness at a heating rate of 20 K/min (b) DSC traces of 1.5 mm $Cu_{46}Zr_{47}Al_7$ BMG at different heating rates for calculating the activation energy for crystallization.

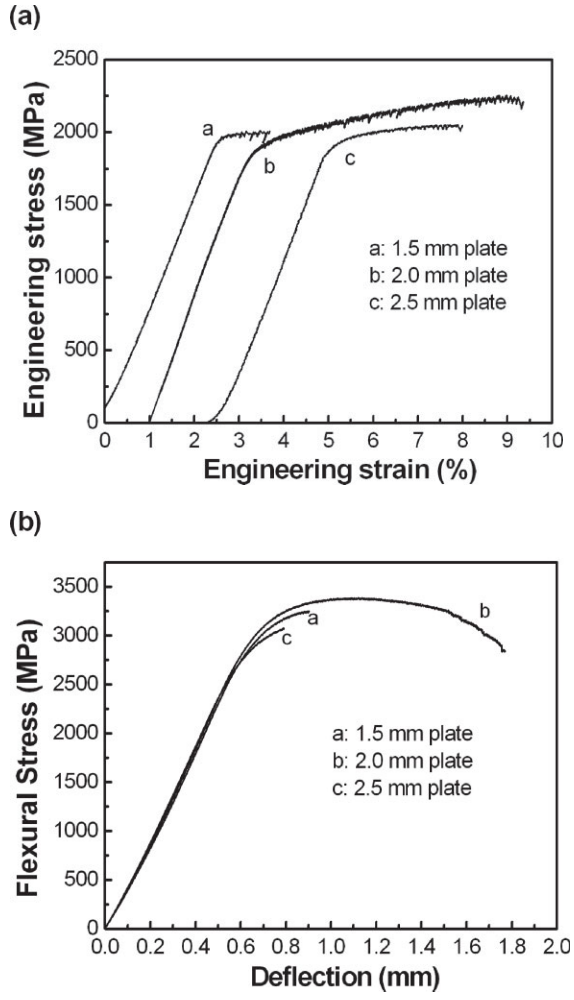

Fig. 5. Mechanical properties of $Cu_{46}Zr_{47}Al_7$ alloys with different thickness (a) Compressive stress–strain curves (b) Flexural stress versus deflection curves, the dimension of bending samples was 20 × 4 × 0.8 mm^3.

 © 2008 WILEY-VCH Verlag GmbH & Co. KGaA, Weinheim

For the three-point bending test, flexural stress was obtained by the following relation:

$$\sigma = 3FL/2wh^2 \quad (1)$$

Here, F is the load, L is the span, w is the width of the sample, h is the height or thickness of the sample. According to the load-deflection ($R \sim \delta$) curves recorded, the flexural stress-deflection curves were obtained, illustrated in Figure 5(b). All of these curves consist of two parts: linear portion (elastic strain) and non-linear portion (plastic strain). Since these samples have the same geometry and loading condition, these bending data will well reflect the difference in their plastic deformation ability. For the three samples with different microstructures, it is clear that they have similar elastic strain limits and different plastic strains prior to failure. The 2.0 mm plate sample has the best plasticity and the 2.5 mm plate sample has the worst plasticity among the three samples.

The deformation features of the lateral surface under compression are shown in Figure 6(a),(c) and (e). For the 1.5 mm plate sample with plastic strain of about 1.2 %, there are fewer visible shear bands on the side surface (see Fig. 6(a)). Figure 6(b) shows dense shear bands on the side surface of the 2.0 mm plate sample. Primary shear bands are inclined at an angle of about 45 degree to the loading direction. The secondary and tertiary shear bands on the deformation surface interact with each other, forming numerous branches. The presence of dense shear bands indicates the good ductility as well as the formation and propagation of multiple shear bands. For the 2.5 mm plate sample, one can find that there are micrometer sized crystalline phases marked "A" in Figure 6(e), acting as obstacles to the local shear deformation. Thus, dense shear bands were activated as meeting the crystalline phases, which may contribute to the enhanced plasticity under compression.

Meantime, the deformation features of the tensile lower surface under bending are shown in Figure 6(b), (d) and (f). For the 1.5 mm plate sample, the shear bands are somewhat straight and sparse (see Fig. 6(b)), which can account for its poor bending plasticity. Besides, it is clear to find the shear bands appear far denser for 2.0 mm plate sample than that for other samples. These shear bands are always wavy, from the SEM observations on the tensile lower surface (as shown in Fig. 6(d)). Those confirm that the 2.0 mm plates sample has better plasticity than other samples. For the 2.5 mm plate, one can find that there are micrometer sized crystalline phases marked "B" in Figure 6(f), acting as obstacles to the local shear deformation, And multiple shear bands were activated as meeting the crystalline phases. However, the stress concentration will induce the grain cracking easily to debase the bending plasticity.

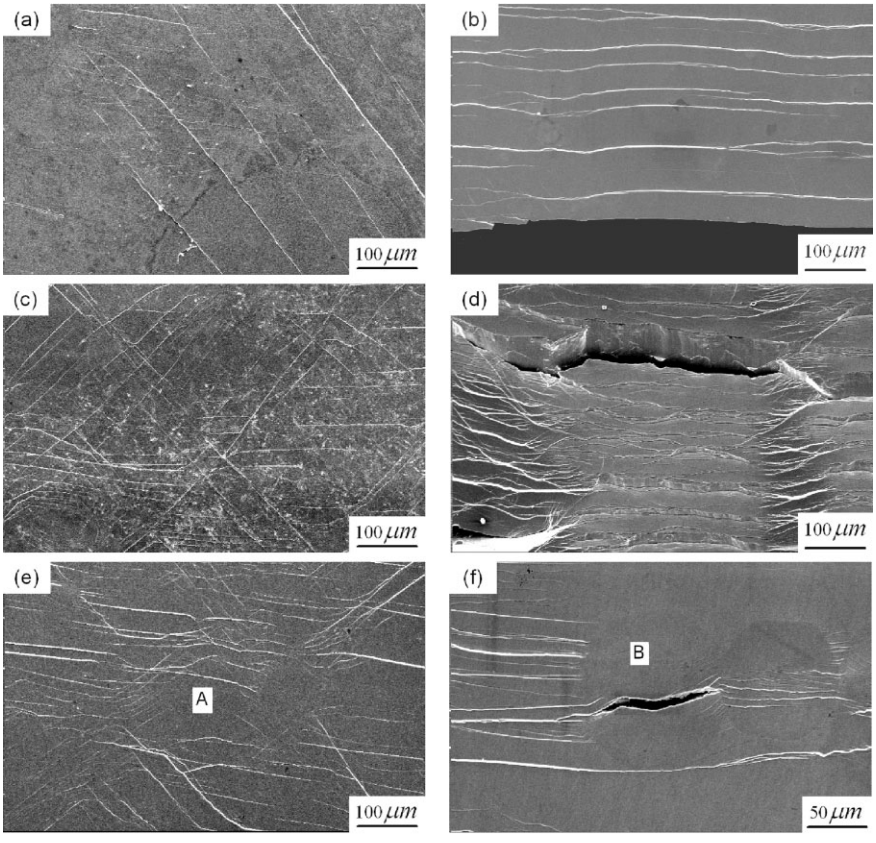

Fig. 6. Deformation features of compressed and bended samples with different microstructures (a, c, e), the shear bands in fracture specimens side surfaces from 1.5, 2.0 and 2.0 mm samples respectively, (b, d, f), the shear bands in tensile side surfaces from 1.5, 2.0 and 2.0 mm samples respectively.

From above results of compression and bending tests, it clearly indicates that the presence of in-situ precipitated small nanocrystals is beneficial to enhance plasticity of the $Cu_{46}Zr_{47}Al_7$ alloy. Deformation-induced nanocrystallization in BMG has been presented in several CuZr based alloys with fully glassy structure, and was used to explain the enhanced plasticity.[17,21] Kumar et al[17] argued that the deformation-induced nanocrystallization in the shear bands during compression was the main reason of the enhanced plasticity for $Cu_{47.5}Zr_{47.5}Al_5$ alloy. Kim et al also claimed that some Cu-Zr based BMGs can display good plasticity, due to the deformation-induced nanocrystallization during quasi-static compression,[21] and proposed that the plasticity of Cu–Zr based BMGs was related with the activation energy of crystallization. In the present study, severe plastic deformation was imposed on the compression sample of 1.5 mm plate with low aspect ratio of 0.7, and a plastic strain of about 70 % was obtained. The DSC curves of these deformed and

 © 2008 WILEY-VCH Verlag GmbH & Co. KGaA, Weinheim

undeformed samples were measured to reveal the possibility of deformation-induced nanocrystallization. Moreover, the surface of deformed samples was measured through XRD. But, we did not observe such a change through our results of DSC and XRD for the deformed samples, either because our DSC and XRD measurements were not sensitive enough or because the alloy has relatively high activation energy for crystallization, about 344 KJ/mol. Where, deformation-induced nanocrystallization can't occur for them during compression. Recent computational simulation had indicated that shear-induced growth of existing nanocrystallites, rather than nucleation of new crystalline regions can take place.[31] Then we conclude that it is the presence of nanocrystal rather than the deformation-induced nanocrystallization that plays a dominant role in enhancing the plasticity of $Cu_{46}Zr_{47}Al_7$ alloys. As for the excellent plasticity of above Cu-Zr-based BMG without nanocrystals,[17,21] it might be related with the free volume introduced during the casting, because these Cu-Zr-based BMGs have small size in diameters of 1 or 2 mm, in which they should contain larger amount of free volume. For example, it is believed that free volume has great effect on the mechanical properties in particular plasticity of prepared BMG alloys.[32,33] The experiment results show that as-cast Ti-based BMG sample with 1 mm diameter has much larger plasticity than that with 6 mm diameter. These are attributed to the higher cooling rate, introducing more defects (free volume).[33] Further research work seems to be desirable about the effect of the free volume on the mechanical properties of these Cu-Zr based alloys.

It is commonly assumed[34–35] that for BMG and BMG composites, fracture initiates when the shear displacement Δu on a particular shear band reaches a critical value, Δu^*. The value of Δu^* depends on the composition of the alloy and the loading conditions. Simultaneously, in response to continuous loading, the additional strain is needed to be accommodated by initiating new shear bands or reactivating new shear banding events on previously formed shear bands. In order to prevent cracking, shear displacement, Δu in a single shear band should be less than the critical valueΔu^*. At the same time, new shear bands should be activated to provide additional strain. Thus, the methods to prevent the single shear band from cracking and promote shear bands multiplication are useful to enhance the plasticity.[36]

The improvement of plasticity of BMG containing small nanocrystals might be due to the several factors which are related with limiting the propagation of individual shear bands and activating new shear bands to provide additional strain. Firstly, nanocrystals which are defect free with high strength, would act as an obstacle to shear band and straight crack. Secondly, the presence of the nanocrystals can introduce stress concentration at the interface of matrix and nanocrystals, which is beneficial to the nucleation, growth, and multiplication of shear bands to provide addition strain. Thirdly, the nanocrystals in the shear band could grow, leading to sharp increase in viscosity and shear delocalization to neighboring undeformed regions with smaller crystalline volume fraction.[37] These all could stop shear deformation of shear band and shear displacement Δu in a single shear band will be less than Δu^* to prevent from cracking. A recent computational analysis of the deformation mechanisms of a nanocrystal-metallic glass composite has indicated the similar viewpoint.[30] Kim et al.[38] have reported a novel finding of slither propagation of shear bands observed at the edge of the fracture surface in a $Cu_{47.5}Zr_{47.5}Al_5$ BMG, containing nanoscale chemical heterogeneities and nanoscale crystals of less than 5 nm in size. This slither propagation of shear bands confirmed the blocking effect of nanocrystals to improve the plasticity. Here, similar experimental evidence is observed on the fracture surface of bending samples as shown in Figure 7. The tension side is dominant for the failure of samples during the bending. The edge of fracture surface of the 1.5 mm sample without nanocrystals is much smooth (inset of Fig. 7(a)). While there are dense small slip steps with nanometer size on the edge of fracture surface of 2.0 mm sample with nanocrystals (inset of Fig. 7(b)). These steps should be related with the nanocrystals to block the propagation of shear bands. At the same time, the offsets or critical shear displacement Δu^* were measured and there were 20 and 45 μm for 1.5 and 2.0 mm samples, respectively. It can be found that the presence of nanocrystals has enhanced the critical shear displacement, comparing with the fully glassy structure. Furthermore, SEM observation shows cores and vein-like pattern are the dominant feature in the shear fracture part which is generally considered to be typical for the quick tensile fracture of BMGs.[39]

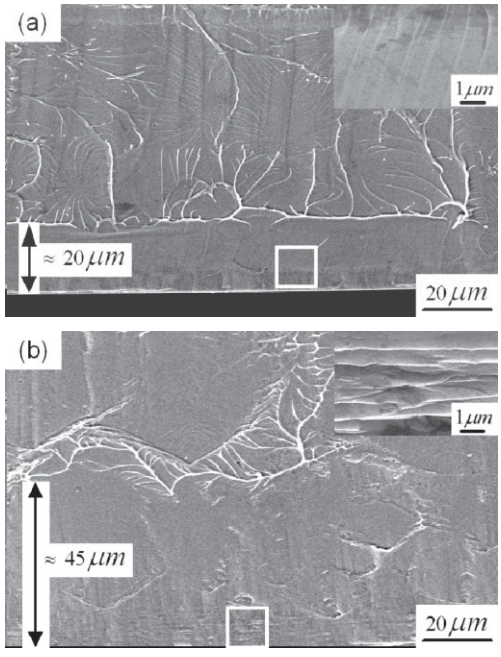

Fig. 7. The fracture surface in tensile side of three-point bending samples, (a) 1.5 mm sample with fully glass structure, (b) 2.0 mm sample containing small nanocrystals. The offsets or shear displacements on the fracture surfaces were measured. Inset shows enlargement of the edges of shear fracture surfaces.

 © 2008 WILEY-VCH Verlag GmbH & Co. KGaA, Weinheim

ADVANCED ENGINEERING MATERIALS

While, for the sample with nanocrystals, river-like patterns and slip steps are the main features. It is obvious that the failure mode has changed from the brittle facture to ductile fracture due to the existence of nanocrystals.

Finally, the 2.5 mm sample has presented a better compression plasticity and poor bending plasticity. During the compression, these CuZr crystallizing phases yield firstly, due to their relatively lower yield strength. Then, dense shear bands were activated as meeting these grains with different size. Similarly, a BMG composite with dendritic precipitates was investigated using neutron diffraction and self-consistent modeling (SCM) was adopted to ascertain its deformation mechanisms. It was shown that the ductile second phase yielded firstly upon loading, and this was followed by multiple shear band formation in the matrix, a process which enhanced the ductility of the composite.[40] It could be found that the present result has a good agreement with their work. Otherwise, many closely spaced shear bands could be found on the deformed sample surface as shown in Figure 6(e). Recently, a group of Cu-Zr and Ti(Cu,Ni)-base ductile work-hardenable BMGs based on 'supercooled martensitic alloys' have been prepared.[28,41] These composites have a good combination of yield strength, plasticity and large size. These are better to meet the requirement as a structure material comparing with their counterpart BMG alloys. However, our bending tests also illustrate these composites containing micrometer sized ductile phase will present poor bending plasticity, because the stress concentration will induce the grain cracking easily.

In summary, we report that $Cu_{46}Zr_{47}Al_7$ alloys with different microstructures including fully glassy structure, marginal BMG containing fine in-situ precipitated nanocrystals and BMG composite containing larger CuZr crystals can be prepared through adjusting the cooling rates during solidification. The investigation of microstructure illustrates that the chemical heterogeneities or nanocrystals observed in Cu-Zr based BMGs could be introduced due to the difference in cooling rate from the edge to the center. The $Cu_{46}Zr_{47}Al_7$ alloy containing small in-situ precipitated nanocrystals has exhibited good plasticity under both compression and bending, while the sample with fully glassy structure only displays poor plasticity. It is clear that the presence of small in-situ precipitated nanocrystals rather than deformation-induced nanocrystallization is beneficial to the enhanced plasticity of $Cu_{46}Zr_{47}Al_7$ alloy. The enhanced plastic deformation ability of the CuZrAl alloy containing small in-situ precipitated nanocrystals is tentatively attributed to the effects of the nanocrystals on the nucleation, growth, multiplication of shear bands and increasing the critical shear displacement.

Received: April 16, 2008
Final version: July 09, 2008

[1] T. Gloriant, A. L. Greer, *Nanostruct. Mater.* **1998**, *10*, 389.
[2] A. Leonhard, L. Q. Xing, M. Heilmaier, A. Gebert, J. Eckert, L. Schultz, *Nanostruct. Mater.* **1998**, *10*, 805.
[3] L. C. Chen, F. Spaepen, *Nature* **1988**, 336, 6197.
[4] C. Fan, R. T. Ott, T. C, *Appl. Phys. Lett.* **2002**, *81*, 1020.
[5] J. C. Lee, Y. C. Kim, J. P. Ahn, H. S. Kim, S. H. Lee, B. J. Lee, *Acta Mater.* **2004**, *52*, 1525.
[6] C. C. Hays, C. P. Kim, W. L. Johnson, *Phys. Rev. Lett.* **2000**, *84*, 2901.
[7] Z. Bian, H. Kato, C. L. Qin, W. Zhang, A. Inoue, *Acta Mater.* **2005**, *53*, 2037.
[8] G. He, J. Eckert, W. Loser, L. Schultz, *Nature Mater.* **2003**, *2*, 33.
[9] G. He, W. Loser, J. Eckert, *Acta Mater.* **2003**, *51*, 5223.
[10] Y. H. Liu, G. Wang, R. J. Wang, D. Q. Zhao, M. X. Pan, W. H. Wang, *Sci.* **2007**, *315*, 1385.
[11] K. F. Yao, F. Ruan, Y. Q. Yang, N. Chen, *Appl. Phys. Lett.* **2006**, *88*, 122106.
[12] J. Schroers, W. L. Johnson, *Phys. Rev. Lett.* **2004**, *93*, 255506.
[13] A. Inoue, W. Zhang, T. Tsurui, A. R. Yavari, A. L. Greer, *Phil. Mag. Lett.* **2005**, *85*, 221.
[14] Z. W. Zhu, H. F. Zhang, W. S. Sun, B. Z. Ding, Z. Q. Hu, *Scr. Mater.* **2006**, *54*, 1145.
[15] J. Das, M. B. Tang, K. B. Kim, R. Theissmann, F. Baier, W. H. Wang, J. Eckert, *Phys. Rev. Lett.* **2005**, *94*, 205501.
[16] K. B. Kim, J. Das, F. Baier, M. B. Tang, W. H. Wang, J. Eckert, *Appl. Phys. Lett.* **2006**, *88*, 051911.
[17] G. Kumar, T. Ohkubo, T. Mukai, K. Hono, *Scr. Mater.* **2007**, *57*, 173.
[18] F. Jiang, Z. B. Zhang, L. He, J. Sun, H. Zhang, Z. F. Zhang, *J. Mater. Res.* **2006**, *21 (10)*, 2638.
[19] F. Jiang, D. H. Zhang, L. C. Zhang, Z. B. Zhang, L. He, J. Sun, Z. F. Zhang, *Mater. Sci. Eng. A* **2007**, *467*, 139.
[20] J. B. Qiang, W. Zhang, G. Q. Xie, A. Inoue, *Appl. Phys. Lett.* **2007**, *90*, 231907.
[21] S. W. Lee, M. Y. Huh, E. Fleury, J. C. Lee, *Acta Mater.* **2006**, *54*, 349.
[22] S. W. Lee, C. M. Lee, J. P. Ahnb, Y. C. Kim, J. C. Lee, *Mater. Sci. Eng. A* **2007**, *449–451*, 172.
[23] W. F. Wu, Y. Li, C. A. Schuh, *Phil. Mag.* **2008**, *88*, 71.
[24] D. C. Hofmann, G. Duan, W. L. Johnson, *Scr. Mater.* **2006**, *54*, 1117.
[25] Y. Yokoyama, K. Fukaura, A. Inoue, *Intermet.* **2002**, *10*, 1113.
[26] F. Jiang, Z. J. Wang, Z. B. Zhang, J. Sun, *Scr. Mater.* **2005**, *53*, 487.
[27] B. B. Sun, Y. B. Wang, J. Wen, H. Yang, M. L. Sui, J. Q. Wang, E. Ma, *Scr. Mater.* **2005**, *53*, 805.
[28] Y. F. Sun, B. C. Wei, Y. R. Wang, W. H. Li, T. L. Cheung, C. H. Shek, *Appl. Phys. Lett.* **2005**, *87*, 051905.
[29] S. Pauly, J. Das, D. C. Duhamel, J. Eckert, *Adv. Eng. Mater.* **2007**, *9*, 487.

 © 2008 WILEY-VCH Verlag GmbH & Co. KGaA, Weinheim

[30] T. Gloriant, M. Gich, S. Surinach, M. D. Baro, A. L. Greer, *Mater. Sci. Forum.* **2000**, *343*, 365.
[31] Y. Shi, M. L. Falk, *Acta Mater.* **2007**, doi:10.1016/j.actamat.2007.11.005.
[32] Y. Liu, H. Bei, C. T. Liu, E. P. George, *Appl. Phys. Lett.* **2007**, *90*, 071909.
[33] Y. J. Huang, J. Shen, J. F. Sun, *Appl. Phys. Lett.* **2007**, *90*, 081919.
[34] R. D. Conner, W. L. Johnson, N. E. Paton, W. D. Nix, *J. Appl. Phys.* **2003**, *94*, 904.
[35] G. Ravichandran, A. Molinari, *Acta Mater.* **2005**, *53*, 4087.
[36] C. A. Schuh, T. C. Hufnagel, U. Ramamurty, *Acta Mater.* **2007**, *55*, 4067.
[37] K. Hajlaoui, A. R. Yavari, A. LeMoulec, W. J. Botta, F. G. Vaughan, J. Das, A. L. Greer, A. Kvick, *J. Non-Cryst. Solids.* **2007**, *353*, 327.
[38] K. B. Kim, J. Das, M. H. Lee, S. Yi, E. Fleury, Z. F. Zhang, W. H. Wang, J. Eckert, *J. Mater. Res.* **2008**, *23 (1)*, 6.
[39] Z. F. Zhang, J. Eckert, L. Schultz, *Acta Mater.* **2003**, *51*, 1167.
[40] B. Clausen, S. Y. Lee, E. Ustundag, C. P. Kim, D. W. Brown, M. A. M. Bourke, *Scr Mater.* **2006**, *54*, 343.
[41] J. Das, K. B. Kim, W. Xu, W. Xu, B. C. Wei, Z. F. Zhang, W. H. Wang, S. Yi, J. Eckert, *Mater. Trans. JIM.* **2006**, *47*, 2606.

 © 2008 WILEY-VCH Verlag GmbH & Co. KGaA, Weinheim